CORA Cork Open Research Archive
Cartlann Taighde Oscailte Chorcaí

Title	Raman scattering spectroscopy of metal-assisted chemically etched rough nanowires
Authors	Glynn, Colm;Lotty, Olan;McSweeney, William;Holmes, Justin D.;O'Dwyer, Colm
Publication date	2011-04
Original Citation	McSweeney, W., Lotty, O., Holmes, J. D. and O'Dwyer, C. (2011) 'Fabrication and Characterization of Single-Crystal Metal-Assisted Chemically Etched Rough Si Nanowires for Lithium-Ion Battery Anodes', ECS Transactions, 35(34), pp. 25-34. doi: 10.1149/1.3567739
Type of publication	Article (peer-reviewed)
Link to publisher's version	http://ecst.ecsdl.org/content/35/34/25.abstract - 10.1149/1.3567739
Rights	© 2011 ECS - The Electrochemical Society
Download date	2026-09-16 19:22:03
Item downloaded from	https://hdl.handle.net/10468/6296

UCC
University College Cork, Ireland
Coláiste na hOllscoile Corcaigh

Raman Scattering Spectroscopy of Metal-assisted Chemically Etched Rough Si Nanowires

C. Glynn[1], O. Lotty[2], W. McSweeney[1], J. D. Holmes[2, 3] and C. O'Dwyer[1]

[1] Department of Physics and Energy, and Materials & Surface Science Institute, University of Limerick, Limerick, Ireland
[2]Materials and Supercritical Fluids Group, Department of Chemistry and the Tyndall National Institute, University College Cork, Cork, Ireland
[3] Centre for Research on Adaptive Nanostructures and Nanodevices (CRANN), Trinity College Dublin, Dublin 2, Ireland

We have shown that SiNWs formed on (100) Si substrates by metal-assisted chemical etching can exhibit different Raman scattering processes that are dependent on the orientation of examined NWs to the incident excitation light. The SiNWs retain the single crystal orientation and doping from the original bulk substrate and form as rough and mesoporous NWs with a SiO_x shell surrounding the NW. The Raman scattering spectra of vertical and horizontally lying SiNWs showed quantum confined phonon scattering processes from narrow and roughened NWs, whose spectral resolution was increased by orienting NW horizontal to the beam to maximize probe cross-section. SiO_x contributions were not evident and specific substrate Raman modes were suppressed for horizontal NWs. Localized beam induced heating to 425 K showed pronounced and specific red-shifting and asymmetry of the TO, 2TO and 2TA phonon modes consistent with phonon quantum confinement effects not observable when the NW were oriented parallel to the incident excitation light.

Introduction

Silicon nanowires (SiNWs), formed by several techniques, have attracted much attention for many applications, such as field effect transistors, nanosensors, and solar cells [1-3]. These applications take advantage of the high crystallinity and/or large surface area of SiNWs. Excitingly, SiNWs have recently been demonstrated as ultrahigh capacity lithium ion battery negative electrodes,[4] which opens up further opportunities for energy storage devices. It has been shown that when crystalline solids are confined to the nanometer range, electron and phonon transport can be significantly altered due to three discrete effects [5] such as increased boundary scattering, changes in phonon dispersion, and quantization of phonon transport. Similarly, theoretical and experimental work [6] has shown that the electrical and thermal conductivities from nanowires differ from those for bulk Si [7]. Furthermore, transport properties are very sensitive to the crystalline lattice characteristics of individual nanowires. Consequently, systematic structural characterization is necessary to distinguish these characteristics.

One method to form SiNWs while maintaining identical crystal structure, growth direction and doping density to that of the bulk Si substrate is to use metal-assisted chemical (MAC) etching [8,9]. This technique involves metal deposition on a silicon substrate from a metal ion containing HF solution causing a localized chemical redox

process in which both anodic and cathodic processes occur simultaneously at the silicon surface. This method can be performed at near room temperature but the major advantage associated with it is the total control over the growth direction and doping levels of the wires formed [10]. The nanowires produced can be tuned in length from a few nanometres to several tens of micrometers and approximately 50-200 nm in diameter [11]. The cores of these Si nanowires are single crystals, and the growth direction has a defined relationship with surface orientation of the wafer used. The anisotropy is not perfect, and the side facets of resulting nanowires can be considerably roughened, most likely due to various surface terminations [12] and bonding characteristics that give considerable variation in etch rates and directions from the same silver catalysed metal assisted etching.

Here, we characterize the Si (100) bulks surface and also NW electrodes fabricated by metal-assisted chemical etching from (100)-oriented bulk Si, using Raman scattering spectroscopy. We have observed that the orientation (vertical or horizontal) of SiNWs influences the phonon scattering processes. In-situ heating through control of incident laser power is also shown to significantly alter thermalized phonon scattering processes occurring in MAC-etched SiNWs even though the NW dimensions are lower than the confined phonon scattering lengths for Si.

Experimental

The NWs, shown in Fig. 1a are fabricated by metal-assisted chemical (MAC) etching of the silicon. To form SiNW layers, 200 mm diameter lightly p-doped silicon (100) wafers (680 μm thickness) with a native oxide layer (approx. 2-5 nm thick) were used as the standard silicon substrate. Each wafer was cut to a size of 5 mm × 10 mm and then cleaned using iso-propyl-alcohol (IPA) before etching. Wafer coupons were sonicated for two cycles in IPA for 20 mins at 40 ^{o}C and dried under nitrogen. Some substrates had polyimide tape protecting the unpolished side during etching reactions. SiNWs were formed using a modified procedure adapted from previous reports [1]. Substrates were immersed for two hours in a heated solution of 10% HF containing 0.04 M $AgNO_3$ and maintained at 50 °C using a thermostated water bath. Upon removal from the etching bath, samples were washed copiously with deionised water and then treated with concentrated nitric acid to remove unwanted silver deposition. The length of the NWs is controlled by the etching time and etchant concentration leaving a uniform, effective porous silicon layer. The remaining skeleton forms a vertical array of NWs ranging from 80 – 200 nm in diameter.

Cleaved {011} cross-sections and (001) surfaces were examined using Hitachi S-4800 and SU70 field emission scanning electron microscopes (SEM). Energy dispersive X-ray analysis (EDX) was conducted using a Hitachi SU-70 FESEM operating at 10 kV equipped with an Oxford Instruments X-max 50 mm^2 solid-state EDX detector. Cross-sectional transmission electron microscopy (TEM) samples were prepared by scraping NWs onto a holey carbon grid and imaged using a JEOL JEM 2100F TEM operating at 200 kV.

Raman spectroscopy was conducted using a Dilor XY Labram spectrometer equipped with an Olympus BX40 confocal microscope and Renishaw InVia Raman spectrometer using a RenCam CCD camera. Excitation was provided by 514 nm ArHe 10 mW green laser with a maximum of 0.512 mW incident power. The spectra are collected with a Peltier cooled CCD detector. The incident power of the laser was adjusted using calibrated filters.

Results and Discussion

Comparison of p-type Si bulk and SiNW layers

Figure 1 shows the resulting SiNW layers that are formed using the metal-assisted chemical (MAC) etching approach described above, and summarized schematically in Fig. 1a. Vertical arrays of NWs are formed across the entire surface of the wafer, as shown in the cross-sectional SEM image in Fig. 1a. High resolution SEM examination reveals that the NWs have an average length of 115 μm. Examination of the top surface of the SiNW layers shows that the wires appear in non-uniform distributions characterized by clumped regions of high density NWs and correspondingly, regions of locally less density (Fig. 1b). Further examination shows that the less dense regions are not devoid of NWs, rather the NWs are bent towards each other forming the high density regions. This stems from a combination of high length-to-width aspect ratio and capillary forces [13] related to the post-etch cleaning procedure. NWs were measured to have an average width of 80 nm, shown in Fig. 1c. TEM analysis in Fig. 1d also confirmed that individual SiNWs are single crystal and electron diffraction measurements also confirm their (100) orientation, consistent with etching from bulk Si(100). The NWs have a characteristic rough morphology consistent with MAC etched NWs in previous reports [13].

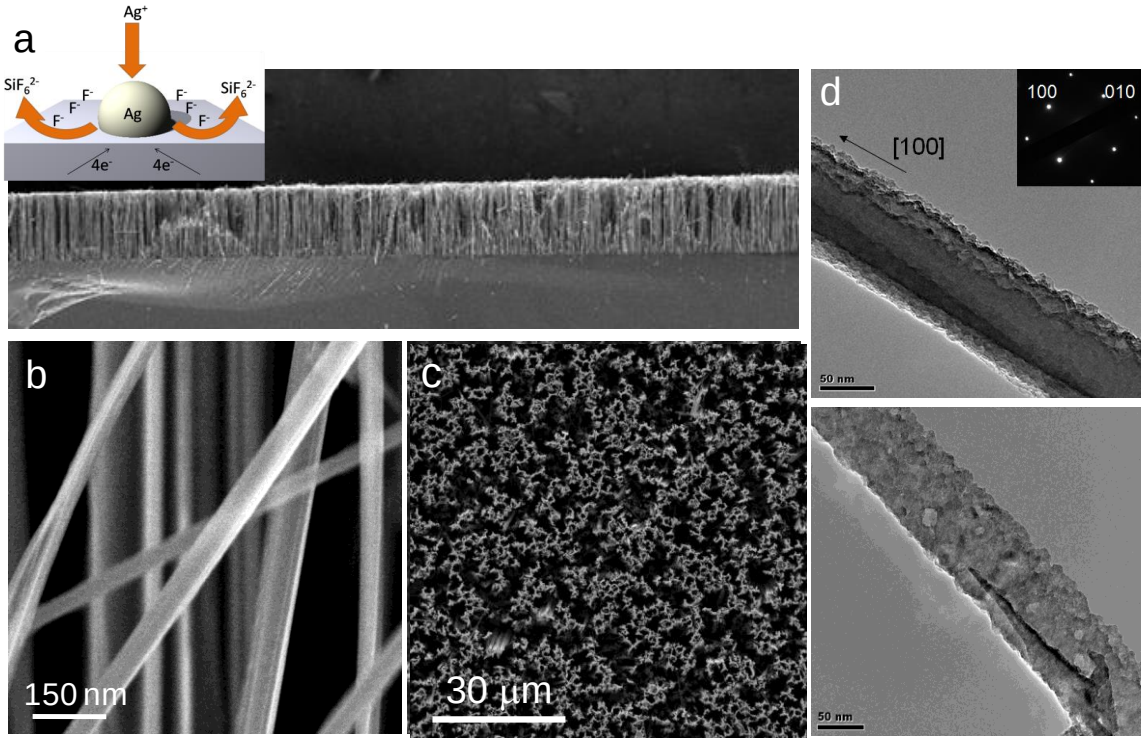

Figure 1 (a) (*Inset*) Schematic of the electroless metal deposition process. Cross-sectional SEM image of the Si NW at low magnification showing the uniformity of the etching depth and NW length. (b) Plan view SEM image of the NW layer and (c) Cross sectional SEM image of several NWs. (d) TEM images of individual nanowires showing the characteristic rough morphology of MAC etched NWs.

Raman spectroscopy was used to characterize the NW layers as a function of their array ordering i.e. diffusely optically reflecting vertically oriented NW regions (v-SiNW)

and comparatively more specularly reflecting horizontally orientated h-SiNW regions, and comparison to bulk Si(100) n and p-type samples. For bulk p and n-type substrates and NWs, Raman spectra were acquired at 514 nm excitation. Raman spectra for the bulk n and p-type Si show only minor shifts in all peaks, which is known to be related to the doping influence on the silicon lattice. Figure 1 shows the Raman scattering spectra from bulk n- and p-type Si and also p-type SiNW layer etched from the p-type bulk Si. The spectra are well defined, and exhibit definite Raman modes for silicon such as and the first order phonon (TO) at ~520cm^{-1} with slight asymmetry indicating optical phonon scattering from crystalline Si, the second order transverse acoustic mode (2TA) and the second order transverse optical phonon band (2TO) at 302 cm^{-1} ~983 cm^{-1} respectively. This latter peak is a convolution of three phonon scattering events giving rise to peaks at 946 cm^{-1} {TO(*X*)}, 970 cm^{-1} {TO(*W*)} and 983 cm^{-1} {TO(*L*)}, and are similar to broad Raman features that are the counterparts of TO–LO pairs in glassy SiO_2.[14] In both bulk Si crystals and SiNWs, the TO + TA combination phonons are also detected at ~670 cm^{-1}. All spectra are plotted with as-acquired intensities, and we attribute the reduced relative intensity of 2TA and 2TO modes to optical scattering and polarization effects in a NW layer that is ~120 μm deep in the ordered matted layer of SiNWs, even though the TO phonon peak for all samples is of similar intensity.

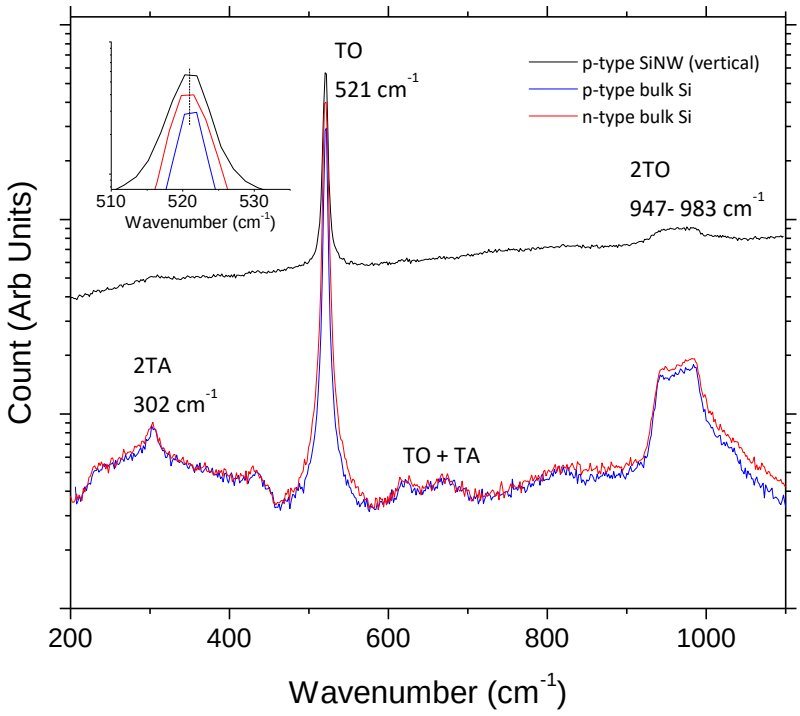

Figure 2 Raman scattering spectra from n- and p-type bulk Si(100) and a vertical array of MAC-etched p-SiNWs. The main phonon scattering modes are identified. (*Inset*) Spectra were collected under identical conditions.

Energy dispersive X-ray analysis of exfoliated SiNWs was conducted to verify the origin of certain Raman scattering processes (scattering or chemically based), such as the presence of SiO_x and remnant elements from the etching process, and their comparison with bulk Si peaks Figure 3 summarises the findings. The spectrum in Fig. 3a identifies the presence of Si, O and C; compared to the bulk Si, the SiNWs are predominantly

coated with SiO_x as shown in the elemental X-ray maps in Fig. 3b where the Si and O are clearly found along the entire length of the SiNW. In fact, the distribution of the oxide is influenced by the roughened surface of the NW and the planar thickness of the oxide is non-uniform. A uniform thickness of oxide would also give a similar elemental X-ray emission map if that uniform oxide was coated on a very rough surface.

Despite optical scattering and convoluted polarization effects limiting the Raman signal contribution from the vertical nanowires, the spectra appear to show the same phonon mode features. Integration of the peak areas for the 2TA phonon peak at 302 cm^{-1} for bulk Si and SiNWs shows that there is significant reduction in the mode intensity after etching to relieve the NWs. The spectral features are maintained and did not change after etching and oxidation (unlike other peaks, as will be shown), which agrees with previous arguments [15] that this peak originates from crystalline Si and not from any SiO_x phase on or underneath the nanowires. As will be shown, localized heating effects did result in a red shift of this mode.

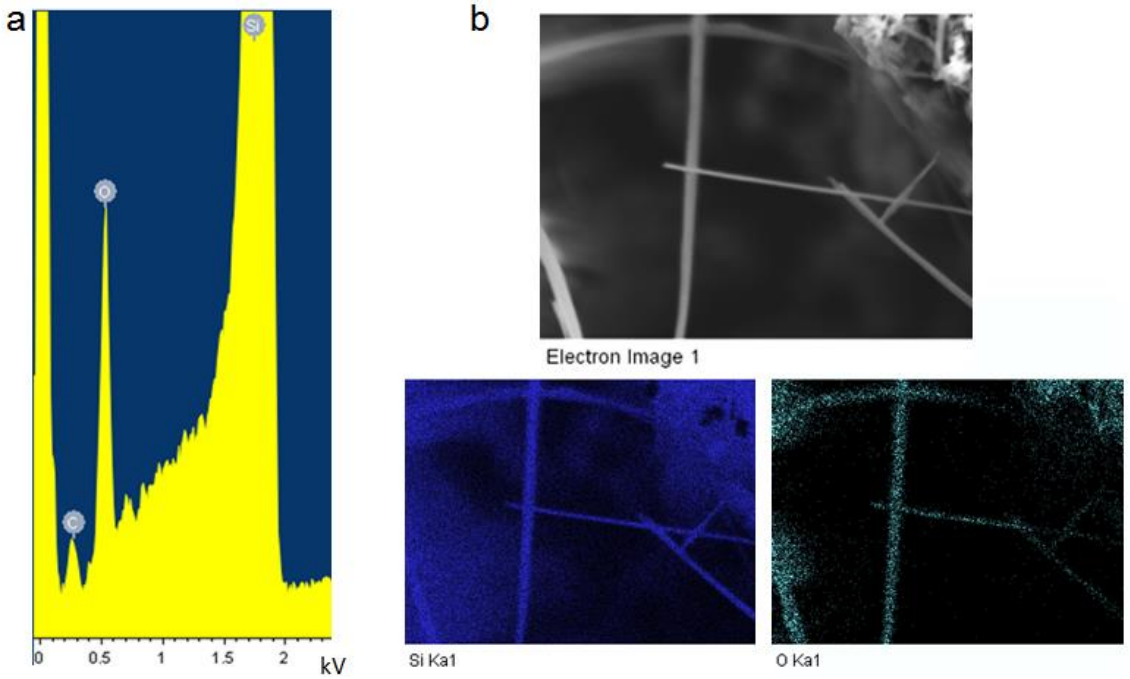

Figure 3 Energy dispersive X-ray (EDX) spectrum from the SiNW layer. (b) Secondary electron image and corresponding elemental maps for Si and O using EDX showing the relatively uniform presence of SiO_x along the length of a SiNW.

Figure 4a shows the Raman scattering spectra for p-type bulk Si(100) and p-type SiNWs from regions where NWs are vertically oriented (v-SiNW) and regions where they are horizontally oriented (h-SiNW), as shown in Figs 4b-d. All spectra show the characteristic phonon scattering modes for Si shown in Fig. 1. Spectra were acquired under identical illumination and collection conditions in order to compare integrated intensities and Raman shifts. There is a noticeable difference in the Raman signals between the two regions: where optical scattering plays a role, the overall baseline intensity is greater but the Raman scattering signal from the SiNWs is reduced stemming from the cross-sectional area probed by the laser beam. For the h-SiNWs shown in Figs 4b and c, the distinction between Raman modes is similar to bulk Si with a measureable broadening of the TO mode and red-shifting of the 2TA and 2TO modes, due to the well-known phonon quantum confinement effect [16,17]. Analysis of the TO mode frequency

shows a very slight (< 1 cm^{-1}) redshift indicating that significant phonon confinement effects are not found from either orientation of NWs. Such confinement can arise from small crystallites within defective NWs [18 or from very narrow diameter NWs via anharmonic vibration effects; neither are found for these ~80 nm wide wires where the temperature is ~300 K (no heating effects due to the laser beam).

We also observe two weak features at 440 cm^{-1} and 620 cm^{-1} which appear also in the bulk Si substrate. After metal-assisted chemical etching to reveal the NWs these features remain; in the h-SiNW regions, their presence is clearly distinguished but they are also found in the v-SiNW regions. Neither of these two modes are due to specificities of the NWs themselves. Although the NWs are relieved through etching, they still comprise the bulk substrate crystal structure and [100] orientation, as shown in Fig. 1d. Those modes are present from the crystalline bulk substrate, as was observed by others [16] and do not come from reported Raman or vibrational modes from nano-SiO_x even though SiO_x surrounds the SiNWs as shown through EDX mapping in Fig. 3.

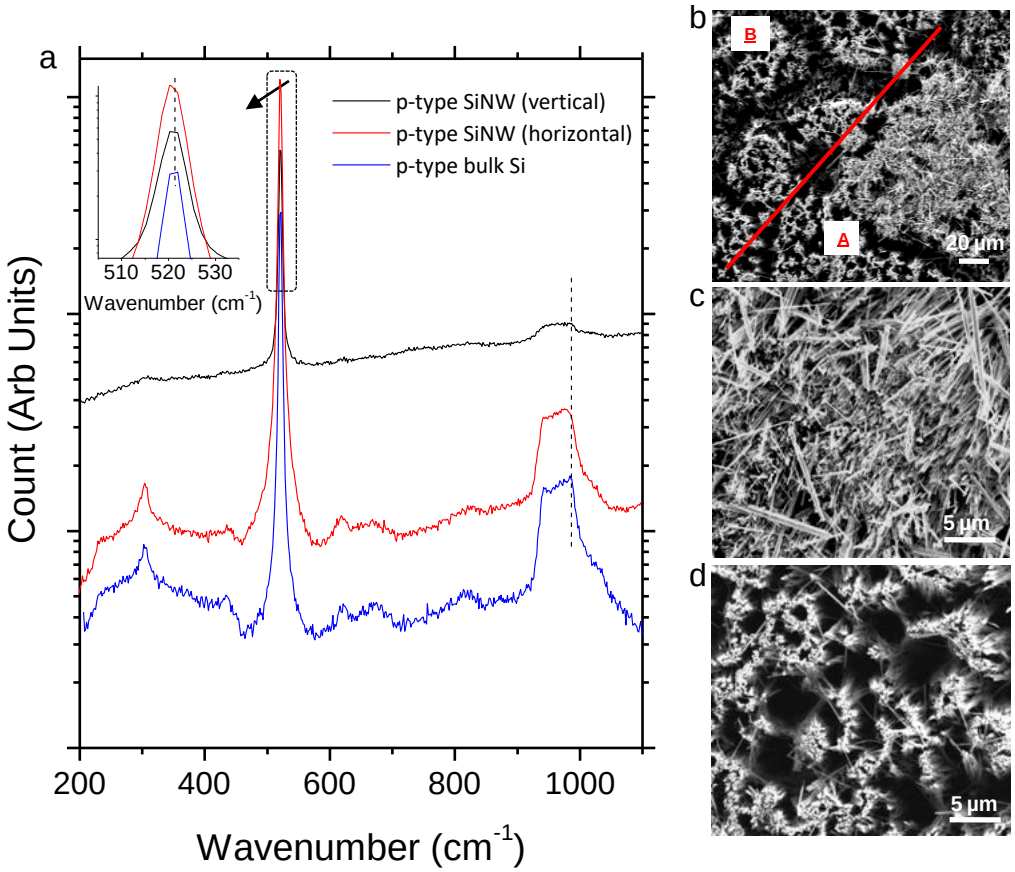

Figure 4 (a) Raman scattering spectra from bulk Si and MAC-etched SiNW layers. Spectra were acquired from regions of v-SiNWs and h-SiNWs. (*Inset*) TO phonon peak showing small (< 1 cm^{-1}) red-shifting of the scattering from NWs compared to bulk Si and also the variations in the 620 cm^{-1} and 670 cm^{-1} modes. (b – d) SEM images of the v-SiNW and h-SiNW regions on the substrate.

To assess the influence of the Raman scattering response from vertical and horizontal bundles of NWs, we conducted line mapping across a region where the arrangement changes from v-SiNWs to h-SiNWs and back to v-SiNWs. Figure 5 shows the resulting spectra. Figure 5a shows the spectra plotted according to Raman scattering intensity, where again the optical scattering and probed cross-section effects are noticed at higher wavenumbers. At laser power densities where no sample heating occurs, we observe that there is consistently a small (1–2 cm^{-1}) wavenumber redshift in the TO phonon scattering as the NW arrangement changes from vertical to horizontal. The surface area of the NW seen by the beam increases and the optical reflectivity due to this lateral surface area also intensifies as seen in the optical image taken from the spectrometer in Fig. 5a.

In Fig. 5b, the TO mode is shown for four of the spectra, as marked in Fig. 5a. We observe the characteristic small redshift from 521 to ~519 cm^{-1} which reverts to 521 cm^{-1} when the spectrum is again taken from the v-SiNWs.

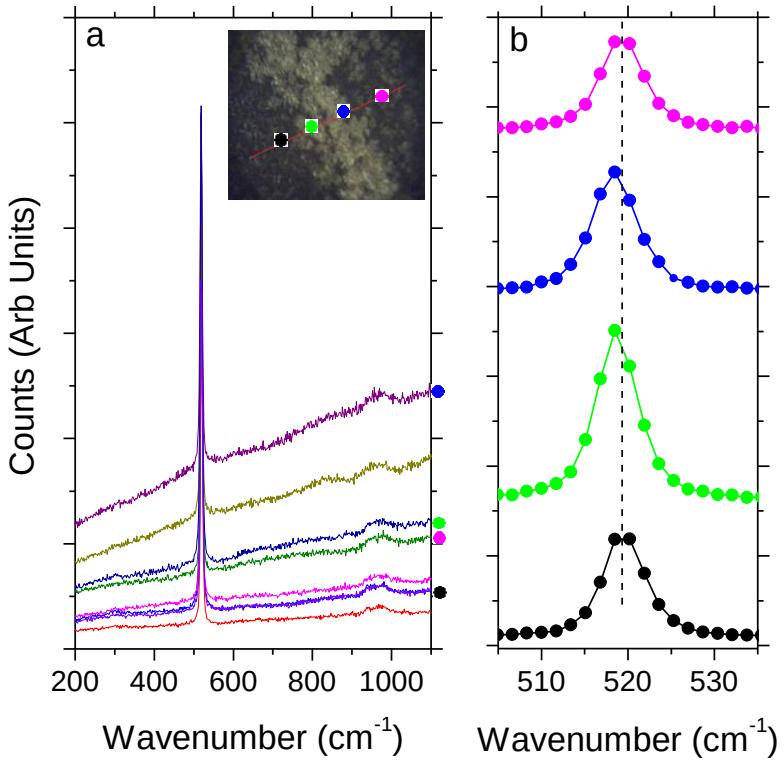

Figure 5 (a) Raman scattering spectra acquired by crossing from regions of v-SiNWs to h-SiNWs and then to v-SiNWs. (*Inset*) Optical image taken from the spectrometer showing the h-SiNWs (light region) and vertical NWs (dark flanking regions) and points of Raman measurements. (b) Variation in TO phonon scattering frequency as a function of position shown in the optical image in (a).

Table 1 summarizes the spectral parameters of the first-order optical phonon (TO) spectra of v-SiNWs and h-SiNWs compared to bulk Si under excitation conditions where no heating occurs. The spectral parameters are the Raman frequency, the frequency shift compared to the Raman frequency of bulk Si, the FWHM, the coefficient of broadening (C_b) defined by $FWHM_{SiNW}/FWHM_{bulk\text{-}Si}$, and the asymmetric coefficient (C_a) defined as LWHM/RWHM, where LWHM and RWHM are the left width at half maximum and the right width at half maximum from the central peak position, respectively. From Table I,

we find that the frequency shift and the coefficient of broadening C_b of v-SiNWs are all larger than those of from h-SiNWs; the asymmetric coefficient C_a however is greater for h-SiNWs. In addition, the asymmetry of the TO peak is less than that from bulk Si. In comparison with the first-order optical phonon peak of bulk Si, the corresponding Raman peak of Si NWs has its frequency only slightly red-shifted, its line-width broadened, and its line shape becomes less asymmetric [16], which is similar to the effect quantum confinement in Si on its Raman spectrum. Orienting NW perpendicular to the beam allows spectra resolution enhancement of crystallinity and surface morphology effects on Raman scattering process to be probed.

The v-SiNWs show uniquely the most asymmetric peak with the widest FWHM. Unusually, the decrease in asymmetry in NWs (vertical or horizontal) compared to bulk Si is different to reports for typically defective VLS of CVD grown SiNWs, but similar to high quality MBE grown wires implying a crystal quality effect that influences phonon confinement.

Samples	Raman Frequency (cm^{-1})	Frequency Red-Shift (cm^{-1})	FWHM (cm^{-1})	C_b	C_a	LWHM (cm^{-1})	RWHM (cm^{-1})
Bulk p-type	521.5	0	4.58	1	2.15	3.13	1.45
SiNW – Vertical	520.1	1.4	5.89	1.28	0.67	2.37	3.51
SiNW - Horizontal	519.7	1.8	5.44	1.19	0.70	2.26	3.18

Table 1: First order phonon (TO) data for p-type bulk Si and corresponding MAC etched vertical and horizontal NWs taken from respective Raman spectra at laser powers where no heating occurred.

Temperature effects on MAC etched SiNW Raman scattering processes

In order to investigate local thermal effects on the Raman processes in SiNWs, spectra were acquired with laser power densities controlled by filters, with three main LDPs corresponding experimentally to 5, 10 and 100% of applied laser power. Experimental annealing temperatures are calculated from Stokes/anti-Stokes components. Thermal effects are insignificant in bulk silicon. Moreover, from the peak positions and cross sections of the Stokes (ω_S) and anti-Stokes (ω_{AS}) components, the temperature of the sample heated by laser radiation can be estimated by the following equation [19,20]:

$$n(\omega_S)I_S = \{n(\omega_{AS}) + 1\}I_{AS}$$

where I_S and I_{AS} are, respectively, the cross sections of the Stokes and anti-Stokes components,

$$n(\omega) = 1/[\exp(\hbar\omega/k_B T) - 1]$$

is the Bose-Einstein thermal factor, T is the sample temperature, and k_B is Boltzmann's constant. The calculated values of the sample temperature are 300 K, 315 K, and 425 K for the samples heated by the laser radiation with a power of 25.5 μW, 51 μW and 0.512 mW, respectively.

Rough SiNWs such as those reported here are excellent thermoelectric materials, having good electrical conductivity and poor thermal conductivity [13]. The thermal conductivity of SiNWs is poorer than that of the bulk silicon due to their lower spatial

dimensions. As the laser power was increased from 25 μW to 0.512mW, the intensity of all phonon modes increased and red shifted. Figure 6 shows the Raman spectra of v-SiNWs (Fig. 6a) and h-SiNWs (Fig. 6b) at 5, 10 and 100% of incident power. Clearly, both the intensity of the phonon scattering mode signals and the resolution of the modes increased significantly. In addition, asymmetric broadening and red shifting of the main TO phonon mode is observed. We also note that red shifting of all modes occurs (2TA, TO and 2TO) with a rounding and profile change observed for the 2TO mode where the 2TO(*X*) becomes dominant and the 2TO(*L*) phonon contribution reduced in relative intensity upon heating.

This observation is markedly different from previous reports by Piscanec *et al.* [21] and others in which they found that serious local heating on the sample even with a power less than 30 mW had a significant effect on the Raman spectra of SiNWs. Related research [22,23] indicates that, when the NW diameter is 20-25 nm and the laser power is 1 mW, the red shift is less than 1 cm^{-1} without obvious asymmetrical broadening. In our case, significant red shifting occurs (~4 cm^{-1}) together with asymmetric broadening for 80 nm diameter wires at <20% of that incident power, linked to the reduced thermal conductivity of the rough SiNWs. The thin and non-uniform oxide coating on the SiNW was insufficiently thick to enhance thermal stability and prevent significant heating effects at low laser power densities.

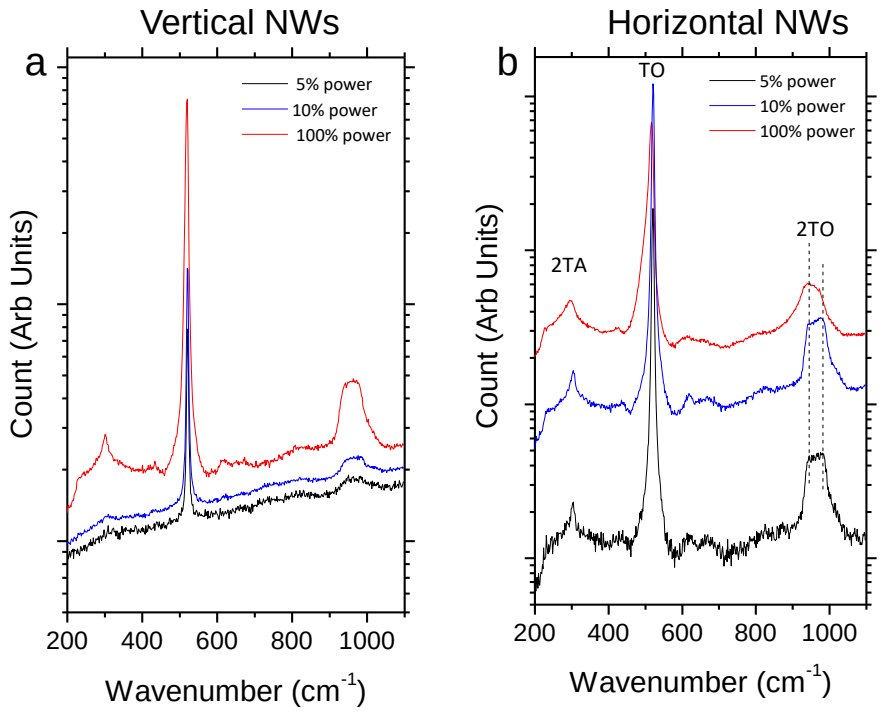

Figure 6 (a) Raman scattering spectra from (a) vertical and (b) horizontal SiNWs as a function of incident laser power. Spectra were acquired at 5, 10 and 100% of incident laser power giving corresponding local heating temperatures of 300, 315, and 425 K.

In comparison with the situation where no heating occurs, Fig. 6 shows that the weak peaks at ~670 cm^{-1} decrease with heating whereas the peak at ~620 cm^{-1} does not. This confirms that the signal at 620 cm^{-1}, which is seen in unheated bulk substrates, does indeed come from the substrate (from which the nanowires are grown) and the ~670 cm^{-1}

peak is a Raman peak from Si stemming from the forbidden (in a perfect infinite crystal) combinatorial phonon mode (TA + TO), which has been observed once from porous Si [16].

Figures 7a and b show the TO phonon for the lowest (25 μW) and highest (0.512 mW) applied laser powers. In comparison with the TO phonon peak of bulk Si, the TO peak of SiNWs at 300 K and 425 K has its frequency down-shifted, its line-width broadened and its line shape becomes asymmetric. These features are accentuated upon heating where the shift is 4 cm^{-1} and the deconvolution of the asymmetric peak shows a contribution at 506 cm^{-1}. These features are expected characteristics of nano-crystalline and porous silicon, which were ascribed to the phonon quantum confinement effect of Si. Therefore, we may identify the spectra in Figs. 7a and 7b as the intrinsic Raman spectra of MAC-etched Si NWs on a bulk Si substrate at room temperature and up to 425 K.

Interestingly, for v-SiNWs, heating induces limited effect and the redshift is the same as the difference between vertical SiNWs at 300 K compared to bulk Si. This implies that anharmonic vibrations that typically arise from variation in the atomic vibration potential energy, become significant at elevated temperature, whereas this is not seen in SiNWs (compared to bulk Si) at 300 K. Anharmonic effects should thus be even more pronounced in horizontal nanowires where the sides of the long axis of the NWs are not parallel. Figure 7a and 7b show this difference; the largest red shift and greatest asymmetry in the TO phonon peak occurs for heated h-SiNWs. Again, negligible shifting is found for unheated v-SiNWs compared to bulk Si, as was also seen in Fig. 1.

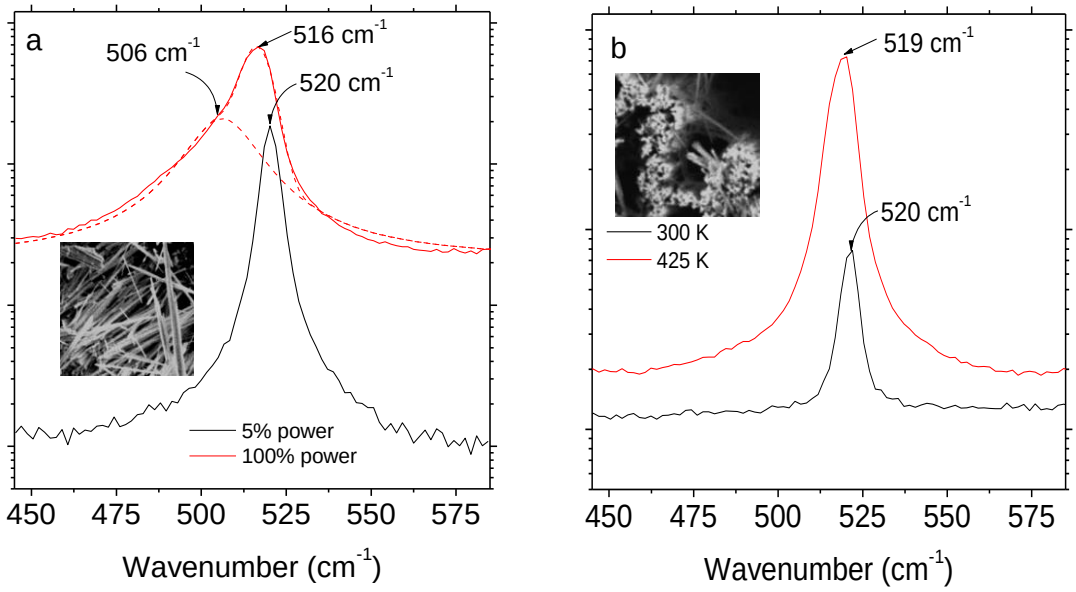

Figure 7 (a) Raman scattering of the TO phonon from (a) v-SiNWs and (b) h-SiNWs as a function of incident laser power. Spectra were acquired at 5, 10 and 100% of incident laser power.

For h-SiNWs, a deconvoluted contribution to the asymmetry in the TO phonon peak is found at 506 cm^{-1}. This deconvoluted band at 506 cm^{-1} is not expected for nanosized diamond cubic Si. It has been shown [24] that this band is due to the presence of hexagonal Si structure. This agrees well with the Raman measurements made on hexagonal diamond Si obtained by nanoindentation [25]. The results are also comparable

to the measurements realized in microcrystalline samples with a mixture of cubic and hexagonal diamond Si phases in agreement with semi empirical models. In our case, contributions at these frequencies due to oxide presence cannot explain the observation of the convoluted band at elevated temperature, despite evidence that a non-uniform oxide is present along the length of all wires investigated.

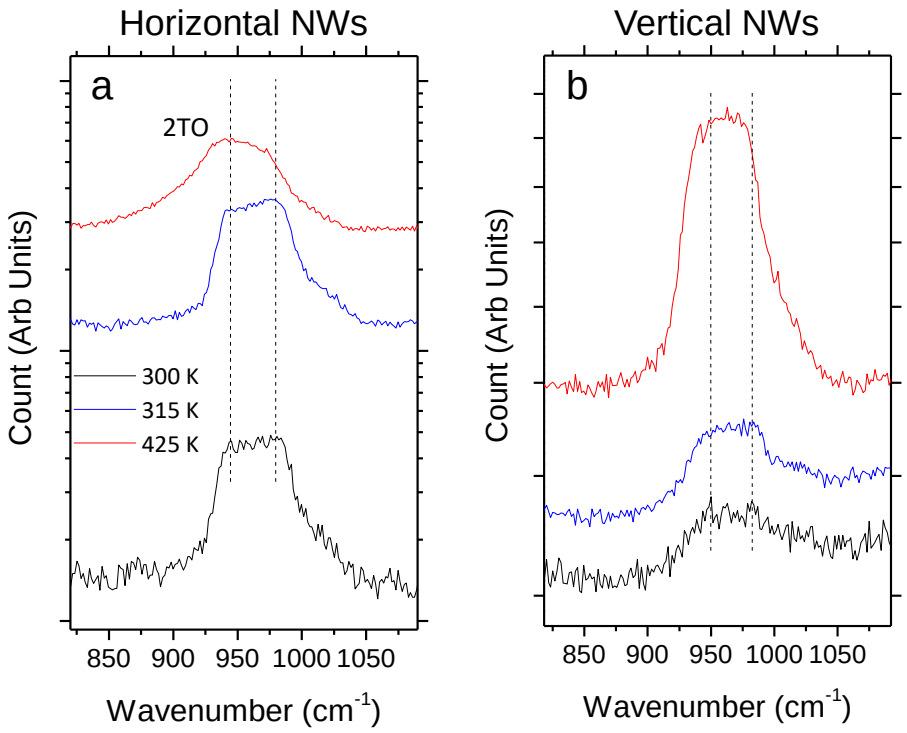

Figure 8 (a) Raman scattering of the 2TO phonon mode harmonic from (a) h-SiNWs and (b) v-SiNWs as a function of incident laser power. Spectra were acquired at 5, 10 and 100% of incident laser power.

Analysis of the 2TO modes, shown in Fig. 8, also show similar effects due to heating and NW ordering. We also note that red shifting of the 2TO mode from horizontal NWs by ~ 6 cm^{-1}occurs due to heating (corresponding to a red shift of ~40 cm^{-1} compared to bulk Si) with an enhancement of the 2TO(*X*) scattering contribution which becomes dominant; the 2TO(*L*) phonon contribution reduces in relative intensity upon heating. For v-SiNWs, the heating induced shift is only 2 cm^{-1} with a shift compared to bulk Si of ~35 cm^{-1}. It has been previously shown experimentally that the correlation length *D* (in nm) of standard diamond cubic Si nanocrystals can be determined from measurement of phonon peak redshift in cm^{-1} and also from the corresponding FWHM in cm^{-1} using the following relations [26]:

$$\Delta\omega = -97.462\left(\frac{0.543}{D}\right)^{1.39}$$

$$FWHM = \frac{2D + 6.2618}{0.81004D - 1.6503}$$

From Raman spectra reported in this work for h-SiNWs at 425 K (where significant red-shifting and broadening of the TO phonon peak was observed), we find almost equivalent values for D; for a red-shift $\Delta\omega$ of 4 cm^{-1}, D = 5.39 and for the corresponding FWHM of 6.34 cm^{-1}, D = 5.24. These values are similar to those reported for diamond hexagonal Si. In that work, a reduction in correlation length was associated with a transformation to standard diamond cubic Si; the correlation length D for our v-SiNWs at room temperature is 3.87 indicative of cubic diamond Si that are known to have smaller D values. While definitive measurements of the Si lattice constants are required, the spectral analysis at higher temperature shows all the hall marks of SiNWs with a slightly different, 'stressed' lattice constant.

It remains to be determined if the MCM model [15] for quantum phonon confinement is the sole cause of the asymmetry, red-shifting and broadening of the TO phonon at room temperature and at elevated temperature. It is possible too that stress effects which can alter the Si lattice constant or the presence of individual Si nanocrystallites within the NWs contribute to these observations. The NWs are single crystal and stem from the very substrate underneath, unlike the majority of SiNW systems grown from CVD or VLS routes. If the confinement is due to crystalline Si features, then it is plausible that the rough features on the SiNW surface act as effective Si crystallites and would have a similar effect to low quality single crystal wires with stacking faults and twin defects or those composed of individual grains which have been shown to down shift phonon scattering frequencies, suggesting a limitation of the phonon mean free path by boundary scattering as opposed to intrinsic Umklapp scattering. This would then account for red shifting of wires that have feature sized greater than the 20-25 nm phonon confinement length.

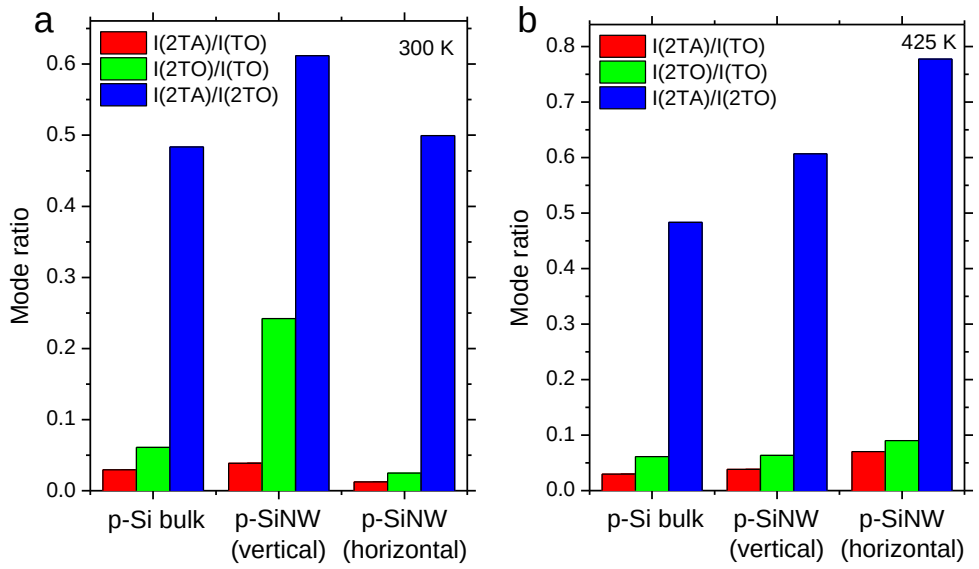

Figure 9 Variation on phonon mode ratios for bulk Si, and v-SiNWs and h-SiNWs at 300 K and at 425 K.

In the present work, we observed that the intensities of the first-order band drops when temperature is increased and the relative integrated intensities of the second-order bands (2TO) and the first-order (TO) mode, which was most pronounced for v-SiNWs at room temperature, remained almost invariant at 425 K (see Fig. 9). All mode ratios are

greatest for v-SiNWs at room temperature, but greatest for h-SiNWs at 425 K; the trend for all ratios from all samples is maintained for a given temperature. The reason for the enhanced intensities of the Raman lines for h-SiNWs, is the higher quantity of the incident photons associated with the increased laser power (larger material cross-section of probed material), resulting in more photon-phonon interactions contributing to the scattering. We ascribe these phenomena to different temperature dependences of the scattering cross-section between the first-order bands and the second-order bands.

In Fig. 9, we can see that the relative intensity I(2TA)/I(2TO) increases, as expected, with greater temperature in cases where a larger physical probed cross-section occurs, *i.e.* horizontal NWs. The acoustic phonon mode seems to have higher scattering efficiency than the optical mode at a higher temperature. In another comparison, the value of I(2TA)/I(2TO) is greatest for the horizontal NWs at 425 K. To understand this observation we take the following consideration. Acoustic bands are typically not found to be influenced by the confinement effect and concurrently, the ratio of the integrated intensities I(2TO)/I(TO) varies with the nanocrystal size, but typically not depend on the heating power densities, *i.e.*, temperature. However, as shown in Fig. 9, this ratio is significantly reduced for vertical NWs at 425 K compared to 300 K and is most likely due to the scattering cross-sections for higher order modes probed by having a greater material cross-section to the incident excitation energy. Thus, heating significantly affects the photon-phonon interaction for SiNWs in MAC etched Si substrates is heavily dependent on the NW orientation, thus implying that Raman measurements of NWs must also consider their orientation to the beam, in addition to other influencing parameters such as crystal purity, crystal structure, NW diameter (for defect free NWs) and grain size (for polycrystalline and defective NWs); to probe quantum confinement inducing features in a SiNW, the resolution is considerably improved when NWs are oriented perpendicular to the beam to minimize optical scattering and polarization effects and increase photon-phonon interaction from all Si (NW diameter, internal defects, grains, crystal structures) and SiO_x phases.

Conclusions

We have shown that metal-assisted chemical etching techniques, used to form 115 µm SiNWs as a vertical array from a bulk (100)-oriented substrate, can exhibit different Raman scattering processes that are dependent on the orientation of examined NWs to the incident excitation light. The SiNWs retain the single crystal orientation and doping from the original bulk substrate and due to uncontrolled Ag^+ decoration of the surface, can form as rough and mesoporous NWs with a SiO_x shell surrounding the NW. The Raman scattering spectra of vertical and horizontally lying SiNWs showed quantum confined phonon scattering processes from narrow and roughened NWs, whose spectral resolution was increased by orienting NW horizontal to the beam to maximize probe cross-section. SiO_x contributions were not evident and specific substrate Raman modes were suppressed for horizontal NWs. Localized beam induced heating to 425 K showed pronounced and specific red-shifting and asymmetry of the TO, 2TO and 2TA phonon modes consistent with phonon quantum confinement effects not observable when the NW were oriented parallel to the incident excitation light.

Acknowledgments

We thank N. Haustrup and Dr G. O'Connor for access to parallel spectral measurements at the National University of Ireland, Galway under the UL-NUIG Alliance. Part of this work was conducted under the framework of the INSPIRE programme, funded by the

Irish Government's Programme for Research in Third Level Institutions, Cycle 4, National Development Plan 2007-2013.

References

[1] Y. Cui, Z. H. Zhong, D. L. Wang, W. U. Wang, C. M. Lieber, *Nano Lett.* **3**, 149 (2003).
[2] M. C. McAlpine, H. Ahmad, D. W. Wang, R. J. Heath, *Nat. Mater.* **6**, 379 (2007).
[3] B. Z. Tian, X. L. Zheng, T. J. Kempa, Y. Fang, N. F. Yu, G. H. Yu, J. L. Huang, C. M. Lieber, *Nature*, **449**, 885 (2007).
[4] C. Chan, H. Peng, G. Liu, K. McIlwrath, X. F. Zhang, R. A. Huggins, Y. Cui, *Nat. Nanotechnol.*, **3**, 31 (2008).
[5] M. S. Dresselhaus, G. Dresselhaus, and A. Jorio, *Annu. Rev. Mater. Res.*, **34**, 247 (2004).
[6] D. Li, Y.Wu, P. Kim, L. Shi, P. Yang, and A. Majumdar, *Appl. Phys. Lett.* **83**, 2934 (2003).
[7] A. I. Hochbaum, D. Gargas, Y. J. Hwang, and P. Yang, *Nano Lett.*, **9**, 3350 (2009).
[8] M. L. Zhang, K. Q. Peng, X. Fan, J. S. Jie, R. Q. Zhang, S. T. Lee, N. B. Wong, *J. Phys. Chem. C.* **112**, 4444 (2008).
[9] K. Q. Peng, Y. Wu, H. Fang, X. Y. Zhong, Y. Xu, J. Zhu, *Angew. Chem. Int. Ed.*, **44**, 2737 (2005).
[10] C. Y. Chen, C. S. Wu, C. J. Chou, T. J. Yen, *Adv. Mater.*, **20**, 3811 (2008).
[11] K. Q. Peng, Y. J. Yan, S. P. Gao, J. Zhu, *Adv. Funct. Mater.*, **13**, 127 (2003).
[12] C. Chartier, S. Bastide, C. Levy-Clement, *Electrochim. Acta.*, **53**, 5509 (2008).
[13] (a) S. W. Chang, V. P. Chuang, S. T. Boles, C. A. Ross, C. V. Thompson, *Adv. Funct. Mater.*, **19**, 2495 (2009). (b) A. I. Hochbaum, R. Chen, R. D. Delgado, W. Liang, E. C. Garnett, M. Najarian, A. Majumdar and P. Yang, *Nature*, **451**, 163 (2008).
[14] S. L. Zhang, X. Wang, K. Ho, Ji. Li, P. Diao, and S. Cai, *J. Appl. Phys.* **76**, 3061 (1994).
[15] I. H. Campbell and P. M. Fauchet, *Solid State Commun.* **58**, 739 (1986).
[16] S.-L. Zhang, Y. Hou, K.-S. Ho, B. Qian, and S. Cai, *J. Appl. Phys.* **72**, 44613 (1992).
[17] B. Li, D. Yu, S.-L. Zhang, *Phys. Rev. B*, **59**, 1645 (1999).
[18] R.-P. Wang, G.-W. Zhou, Y.-L. Liu, S.-H. Pan, H.-Z. Zhang, D.-P. Yu, Z. Zhang, *Phys. Rev. B*, **61**, 16827 (2000).
[19] M. Balkanski, R. F. Wallis, and E. Haro, *Phys. Rev. B* **28**, 1928 (1983).
[20] S. D. Rassat and E. J. Davis, *Appl. Spectrosc.* **48**, 1498 (1990).
[21] S. Piscanec, M. Cantoro, A. C. Ferrari, J. A. Zapien, Y. S. Lifshitz, T. Lee, S. Hofmann, J. Robertson, *Phys. Rev.* B, **68**, 1 (2003).
[22] Z. Su, J. Sha, G. Pan, J. Liu, D. Yang, C. Dickinson, and W. Zhou, *J. Phys. Chem. B*, **110**, 1229 (2006).
[23] Y. Chen, B. Peng, and B. Wang, *J. Phys. Chem. C*, **111**, 5855 (2007).
[24] A. Fontcuberta i Morral, J. Arbiol, J. D. Prades, A. Cirera, and J. R. Morante, *Adv. Mater.* **19**, 1347 (2007).
[25] G. Weill, J. L. Mansot, G. Sagon, C. Carlone, and J. M. Besson, *Semicond. Sci. Technol.* **4**, 280 (1989).
[26] G. Viera, S. Huet, and L. Boufendi, *J. Appl. Phys.* **90**, 4175 (2001).